Systematic effects in coherence peak and phase evaluation of signals obtained with a vertical scanning white-light Mirau interferometer

Peter Lehmann*, Mahr GmbH, Göttingen, Germany

ABSTRACT

Optical profiling based on vertically scanning white-light interferometry is a well established 3D measuring technique for more than one decade now. In recent years the area of application of these instruments tends more and more from laboratory to industrial applications, where robustness, compactness, and cost efficiency is required. A new instrument developed on the basis of a Mirau interferometer with a microscopic field of view meets important requirements of industrial use. Surface heights can be obtained with subnanometer resolution and the measuring setup is less sensitive to vibrations, so that roughness measurements on optical surfaces are possible even in a harsh environment.
However, principal limitations arise in certain applications, e.g. if optically smooth surfaces with either flanks, curvatures, edges, or grooves are to be measured. This contribution deals with phenomena, which become relevant in these cases. The occuring effects lead to differences in the results of coherence peak and phase analysis of the interference signals, and therefore may be the origin of ghost steps in the measuring results.

Keywords: White-light interferometry, optical profilometry, Mirau interferometer, surface slope, coherence peak, phase evaluation, dispersion

1. INTRODUCTION

Optical profiling shows several advantages over tactile sampling by use of stylus instruments. First of all the measuring principle is contactless, so that damaging of the object's surface is avoided. By use of an areal imaging camera the height values within the field of view can be obtained in parallel. Therefore, the measuring process is less time consuming compared to point-wise measuring methods, either optical or tactile.
Especially with interferometric methods a highly resolved height measurement is achieved even for larger measuring areas. If the phase information is utilized a longitudinal resolution of less than one nanometer is reached, which is comparable to or even better than the resolution of phase-shifting interferometers.[1]
On the other hand, if white-light light is used, even rough engineered surfaces can be measured, based on the evaluation of the coherence peak position. This is obtained from a so-called vertical scan or depth scan, where the optical path length difference between measuring and reference beam is varied over a well-defined measuring range and interferograms are captured by a CCD camera for various scanner positions.[2]

2. SENSOR DESIGN AND SETUP

Fig. 1 shows a scheme of a topography sensor based on the principle of scanning white-light interferometry (SWLI). A LED-based light source is used in order to keep the dimensions of the sensor small and to avoid thermal impacts. The interferometer is integrated in a compact Mirau microscope objective. This results in a robust setup, which is easy to adjust. A digital CCD camera is used to renounce a frame-grabber and to obtain a higher frame rate compared to conventional video systems. During the measuring process the Mirau objective is scanned along the optical axis by use of a piezo positioning system, while at equidistant axis positions white-light interferograms are captured by the CCD. The distance covered by the objective between two consecutive frames is typically 50 – 100 nm, if high measuring accuracy is required.

* peter.lehmann@mahr.de; phone +49 (0)551 7073-568; fax +49 (0)551 7073-421; www.mahr.com

Optical Micro- and Nanometrology in Microsystems Technology, edited by Christophe Gorecki, Anand K. Asundi, Wolfgang Osten, Proc. of SPIE Vol. 6188, 618811, (2006) · 0277-786X/06/$15 · doi: 10.1117/12.660892

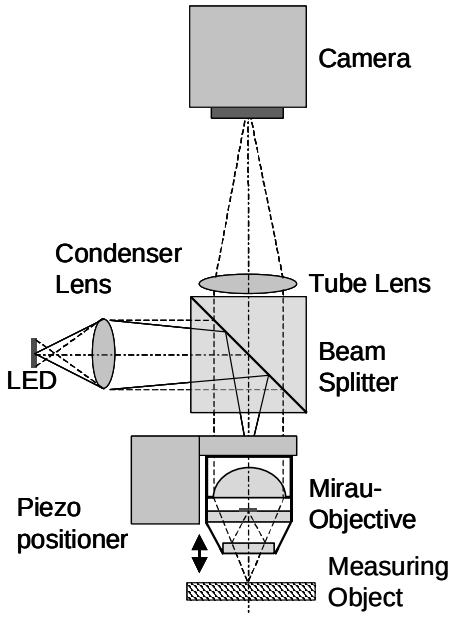

Figure 1: Schematic setup of the Mirau-type white-light interferometer.

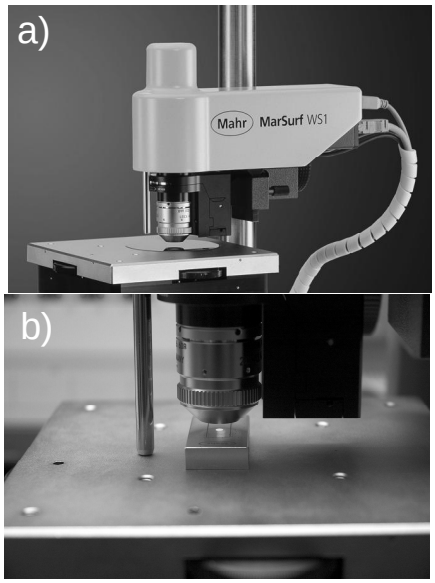

Figure 2: a) Photograph of the compact SWLI sensor, b) detailed view: Mirau objective, measuring object with illuminated field of view, and vibration damping rod.

Fig. 2 a) is a photograph of the complete sensor, which was developed through cooperation of the company Mahr with the Institut für Technische Optik (ITO) of the University of Stuttgart, Germany. Fig. 2b shows a 20x Mirau-objective with a numerical aperture of 0.4, the illuminated spot on the surface of the workpiece under investigation and a steel rod, which connects the interferometer with the object stage in order to keep the measuring loop small. This is used to avoid disturbances caused by vibrations and therefore to enable high-resolution measurements without any further vibration isolation equipment even if the measuring system is situated close to a production line.
The sensor meets some important requirements of manufacturers of engineered surfaces. In order to realize an as large as possible field of view and small sensor dimensions a rather short focal length of 80 mm of the tube lens has been chosen. As a consequence of the large field of view and the limited pixel number of the camera used in order to achieve a maximum frame rate a (lateral) oversampling is no longer possible. Hence, a proper signal analysis has to be performed in order to avoid measurement errors.

3. SIGNAL PROCESSING

In general, signal processing in vertical scanning white-light interferometry is performed in several steps.[1,3,4,5] First, the height position, where the envelope or coherence peak occurs, is determined either by contrast analysis or by slope determination in the frequency domain. In addition, a phase value is estimated for the signals from each camera pixel in order to achieve an accuracy comparable to conventional phase-shifting interferometry (PSI). Our results of computer simulations exhibit, that for a certain signal-to-noise-ratio SWLI with phase evaluation shows a better accuracy than PSI. The reason for this is a greater number of sample points of the interference signal used in SWLI compared to conventional PSI, where the phase information is typically obtained from only four or five intensity values.[1] A further advantage of SWLI in comparison with PSI is, that the axial measuring range is not limited by the focus depth but only by the total height range covered by the scanning unit.
Nevertheless, there are several applications especially in the field of MEMS/MOEMS and optics measurement where the accuracy achievable with coherence peak evaluation is not satisfying. On the other hand, phase evaluation alone leads to 2π ambiguities as soon as the surface height differences exceed half the central wavelength of light. This problem can be solved by an unwrapping procedure, where the height difference attributed to neighboring pixels is assumed to be less than $\pm \lambda/4$. However, this procedure generally fails, if height steps or steeper flanks are present on a measuring object.
Therefore, several approaches have been made, which try to get rid of the problem of phase ambiguity by determining the fringe order using the height information provided by the coherence peak.[1,3,4,5] The algorithm used within the context

of this paper is similar to the procedure described by Fleischer et al.[3] and leads to a highly resolved coherence peak and phase evaluation based on a minimum computational effort.
Another point, that should be mentioned here, is the sensitivity of the evaluation procedure to the ambient conditions during measurement. Fig. 3 shows measuring results, which were obtained in a harsh environment, i.e. the measuring instrument was put on a simple office desk in the first floor of a vibrant building with no further vibration isolation except for the vibration damping rod shown in Fig. 2 b). The measuring object was a flat diamond milled aluminium surface. In Fig. 3 a), where the result of the coherence peak evaluation is shown, the nano-structure caused by the diamond milling process as well as the grain boundaries of the aluminium can be observed. However, a superimposed fringe structure can be found in this result of coherence peak evaluation. This is a consequence of the interference fringes in combination with the remaining vibrations during measurement. The effect can be eliminated, if the phase evaluation technique is applied, as it is shown by Fig. 3 b). The surface height differences resulting from the manufacturing process are found in a total height range of 30 nm.

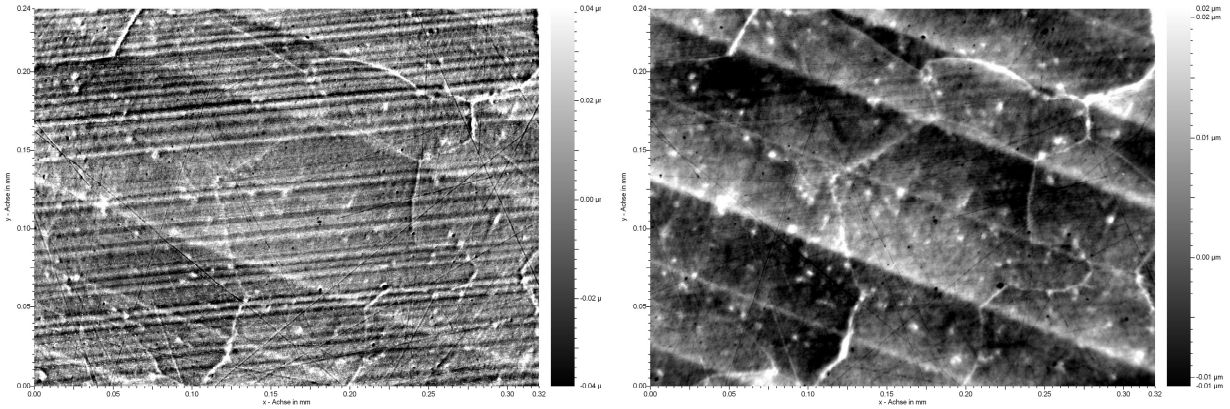

a) **b)**

Figure 3: 3D-topography of a diamond milled aluminium laser mirror measured by use of the instrument shown in Fig. 2 a) with a 50x Mirau objective (numerical aperture 0.5) resulting in 0.32 x 0.24 mm^2 field of view, a) obtained by coherence peak evaluation (total height range shown: 80 nm), and b) obtained by phase evaluation (total height range shown: 30 nm).

4. LIMITATIONS OF SWLI

SWLI signal processing techniques, which are based on a combination of the coherence peak evaluation for fringe order determination followed by a phase evaluation resulting in an accurate height measurement require, that the difference between the height value obtained from the estimated position of the coherence peak and the height value corresponding to the estimated phase value is less than one quarter of the central wavelength used for illumination.

4.1 Batwings

This assumption may be violated if the measuring object shows a structure with height steps as they are typical for micro-systems technology or if steeper flanks are to be measured. In the first case interference of light rays reflected from different height levels accompanied by diffraction phenomena can be shown to give rise to so called batwings in the profiles obtained on the basis of the coherence peak position.[6] Fig 4 a) shows the result of the envelope evaluation for a chromium grating on a glass substrate. Batwings occur at the edges of the rectangular microstructures and become visible as bright or dark stripes in Fig. 4 a). Note that the occurrence depends strongly on the position within the field of view. Generally, in situations, where dominant batwings occur, which are smaller than a quarter of the mean wavelength, a phase analysis may be applied in order to make the evaluation independent of this effect.[4] If the heights of the batwings exceed a quarter of the mean wavelength even the results of phase analysis exihibit the batwing effect (see Fig. 4 b). Phase unwrapping procedures in combination with a sophisticated step height estimation are necessary in order to remove the batwings and to determine the step height of 80 nm correctly, as it is shown in Fig. 4 c). As soon as the step height is of the same order of magnitude as the coherence length of the white light or even greater, this kind of interference is no longer possible and the batwing effect disappears.[6]

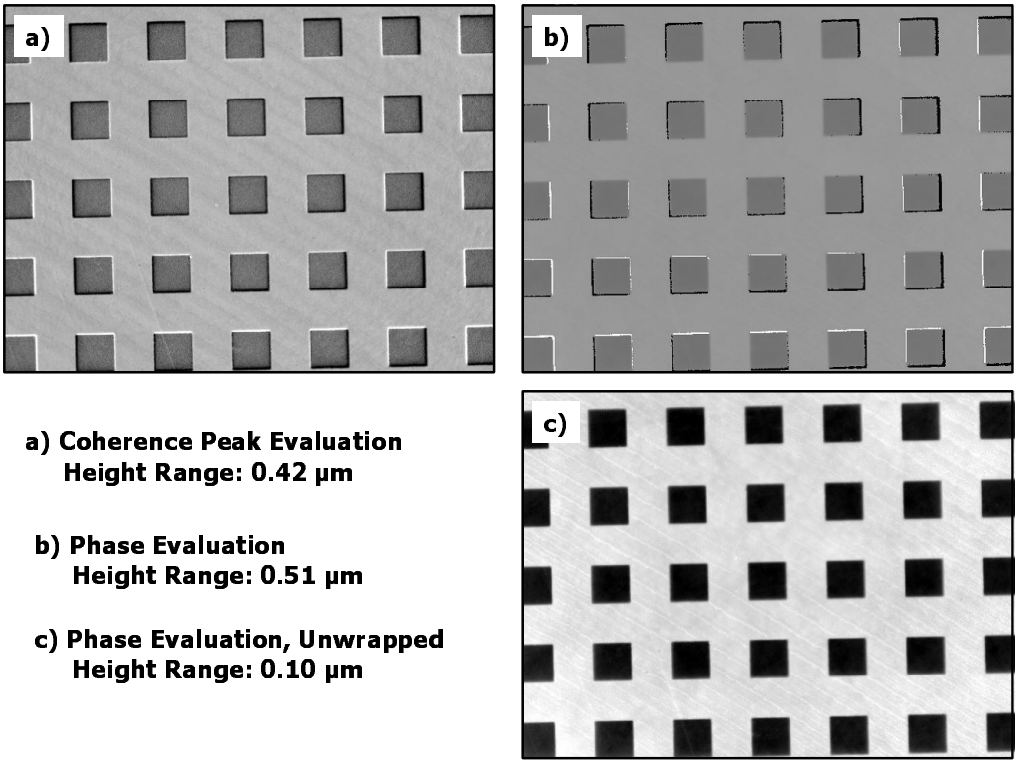

Figure 4: a) 3D topographies of a grating structure with rectangular cavity of 80 nm depth, field of view 0,32 x 0,24 mm^2.

4.2 Surface Slope Effects

However, there are further cases, where systematic deviations of corresponding height values obtained from the coherence peak and phase analysis occur. Consequently, 2π phase jumps may emerge in these cases, if the fringe order is obtained from the coherence peak position.

An example of a sinusoidal surface profile is illustrated in Fig. 5. Results of the coherence peak evaluation (a), the phase evaluation based on fringe order determination by use of the coherence peak results (b), and finally the phase evaluation resulting, if an unwrapping algorithm is applied (c) are shown. In Fig. 5 b) some ghost steps oriented parallel to the flanks of the sinusoidal structure can be observed. For further analysis of these ghost steps Fig. 6 a) shows single sinusoidal profiles obtained from only one single line of the CCD matrix by envelope, phase and unwrapped phase evaluation.

The differences between the results of coherence peak and the unwrapped phase evaluation according to Fig. 6 b) show a systematic behavior, depending on the sinusoidal shape and the position within the field of view. The mean wavelength of the used LED illumination was 620 nm. Hence, the maximum difference between coherence peak and phase position, which can be tolerated in order to avoid ghost steps is ± 155 nm. In those regions in Fig. 6, where this value is exceeded, ghost steps occur in the usual SWLI phase evaluation according to Fig. 6 a), middle curve. Note that the maximum slope of the sinusoid (1,8°) is rather moderate.

Although these ghost steps can be easily eliminated by an unwrapping algorithm as it is shown in Fig. 6 a), bottom curve, this procedure is not quite satisfying, since one of the advantages of white-light interferometry, namely the signal evaluation for each pixel separately, is lost, if unwrapping is performed.

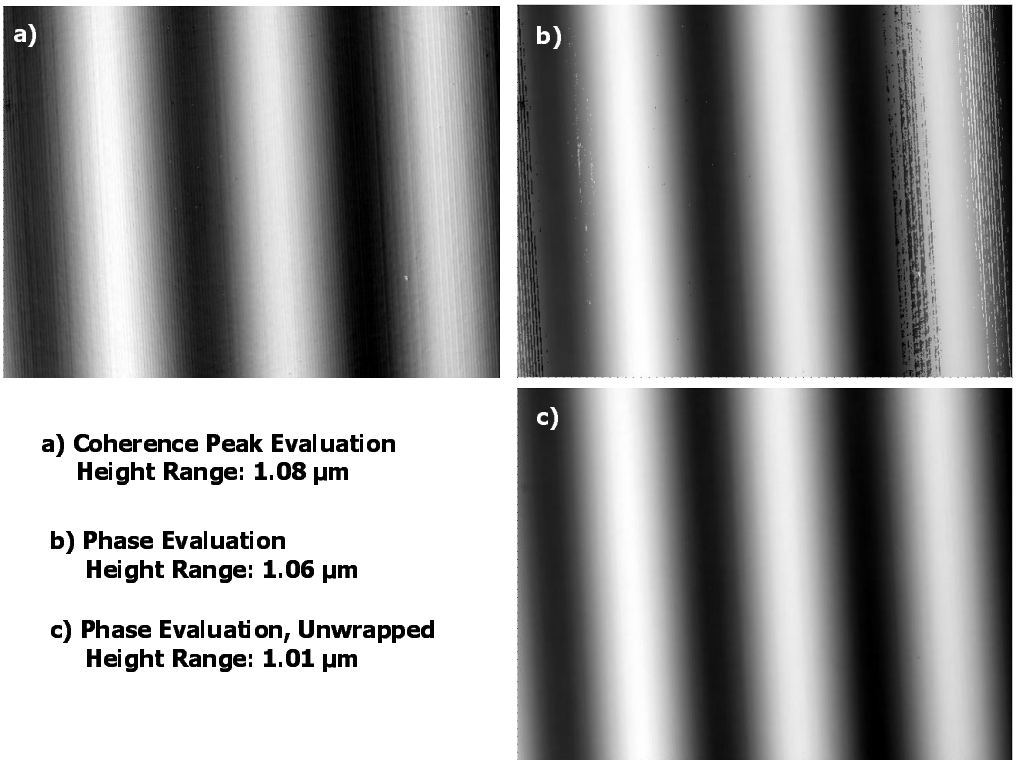

Figure 5: a) 3D topographies of a sinusoidal surface (0.5 µm amplitude and 100 µm period length), field of view 0,32 x 0,24 mm^2.

5. ANALYSIS OF SLOPE EFFECTS

In this section the origin of these systematic differences between phase and coherence peak position is analyzed. First, in Fig. 7 a) two signals (corresponding to x-axis position 665 and 707 µm in Fig. 6) are chosen, which show the same phase value, but a maximum positive or negative difference between the results of the (unwrapped) phase evaluation and the coherence peak evaluation. The two signals according to Fig. 7 b), top diagram, exhibit the same frequency and phase value but the corresponding contrast curves (Fig. 7 (b), bottom diagram) show, that the positions of the envelope are clearly different for these signals. Consequently effects, that result from an effective numerical aperture, which depends on the local tilt angle of the object's surface can be excluded.[7]

Another reason for ghost steps documented in the literature in context with Linnik and Michelson interferometers is an unbalanced wedge dispersion in a real cube beam splitter.[8,5] Dispersion leads to a change of the group velocity of the electromagnetic waves, whereas the phase velocity nearly remains unchanged. The change in the group velocity influences the position of the coherence peak.[1,8] On the other hand, the phase difference between object and reference wave is influenced by the phase velocity, and therefore phase analysis leads to the optical path length difference as long as the central wavelength of the white-light is taken into account. Therefore, the surface shape obtained from phase evaluation is generally closer to reality than the shape obtained from the coherence peak position.[4, 2, 9]

Although a Mirau interferometer doesn't comprise a cubic beam splitter, there are other sources that may lead to dispersion effects. Fig. 8 a) illustrates a simplified scheme of a Mirau objective. After having passed the last lens of the objective the object rays pass two plane parallel glass plates, first the holder of the reference mirror, and second the beam splitter, and after being reflected from the object's surface the other way round. The reference rays pass the plate with the reference mirror two times before and two times after being reflected by the mirror. Hence, if the thickness of these two parallel plates is the same and the surface of a plane measuring object is perfectly aligned with respect to the reference surface, both, measuring and reference rays travel the same length in glass and consequently the dispersion for two corresponding rays should always be the same.

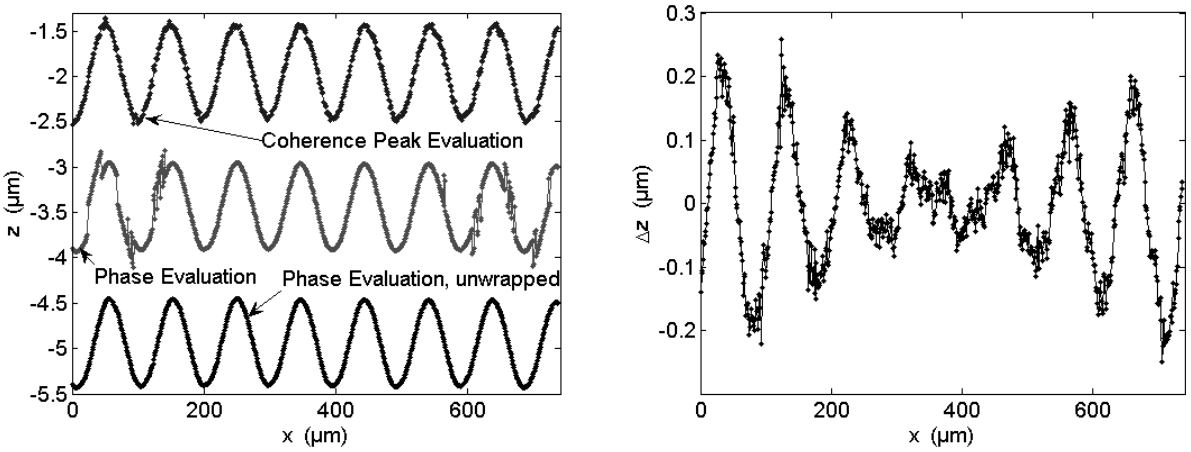

a) **b)**

Figure 6: a) Sinusoidal profiles with 0.5 µm amplitude and 100 µm period length obtained from a single line of the CCD by coherence peak evaluation only ((a), top), from coherence peak evaluation followed by phase evaluation ((a), middle), and phase evaluation followed by phase unwrapping (a), buttom), and b) difference between coherence peak and unwrapped phase evaluation by use of a 20x/0.4 Mirau objective.

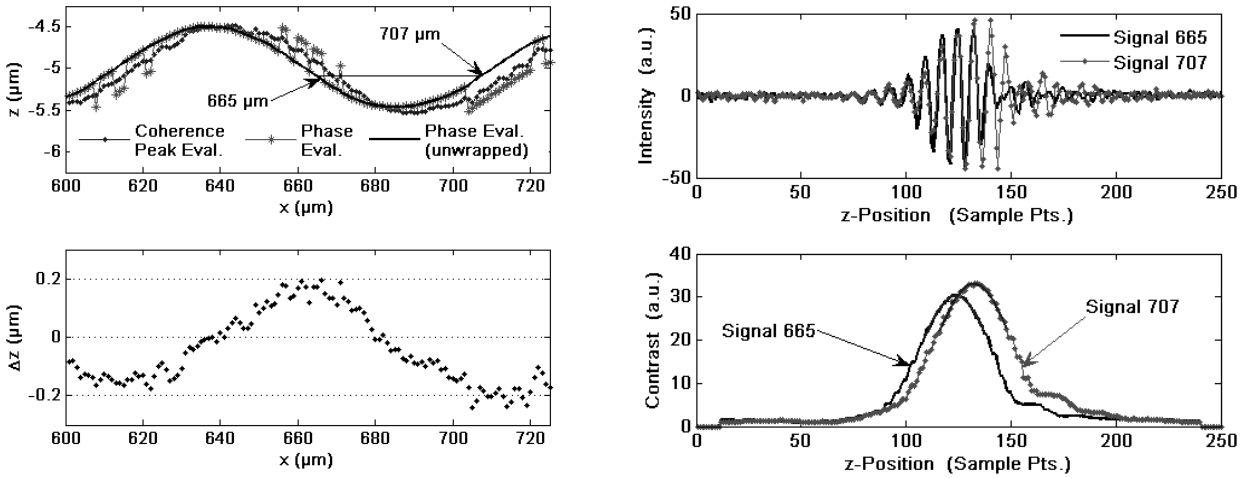

a) **b)**

Figure 7: a) top: detail of Fig. 6 a) showing the results of coherence peak, phase, and unwrapped phase evaluation, bottom: corresponding difference between coherence peak and unwrapped phase evaluation, b) interference signals according to x-axis position 665 and 707 µm, b), bottom: result of contrast (i.e. coherence peak) evaluation for the signals shown above.

The situation is different, if the surface of the measuring object is tilted with respect to the reference plane as it is shown for an unfolded ray path and an on-axis point in Fig. 8 b). Obviously the mean traveling length in glass is longer and therefore, the effective dispersion of the measuring light cone compared to the reference light cone is greater. Fig. 8 c) shows the same for an off-axis point close to the edge of the field of view in direction of positive surface slope. In this case the mean traveling length in glass is shorter and therefore, the effective dispersion of the measuring light cone compared to the reference light cone is significantly smaller. Finally, in Fig. 8 d) the opposite situation is illustrated, where an off-axis point in negative direction is examined. The ray cones are similar to those shown in Fig. 8 b). The effective dispersion becomes greater as the tilt increases, until some edge rays hit the tilted measuring surface perpendicularly. For these rays the dispersion is considerably smaller, and consequently the effective dispersion

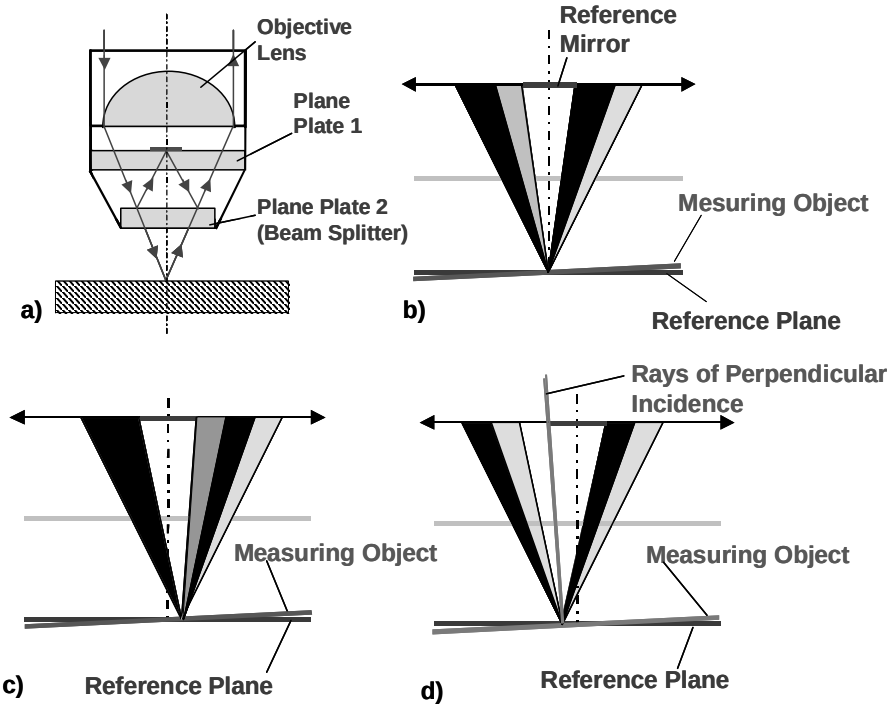

Figure 8: a) Scheme of the Mirau microscope objective, b) unfolded ray cones of both, measuring and reference rays (black areas) and regions, where only reference rays occur (gray areas) for an on-axis point, c) unfolded ray cones of both, measuring and reference rays (black areas), a region, where only measuring rays pass through (dark gray area), and a region of only reference rays (gray area) for an off-axis point in positive slope direction, d) unfolded ray cones of both, measuring and reference rays (black areas) and regions, where only reference rays occur (gray areas) for an off-axis point in negative slope direction.

decreases. In order to quantify these effects theoretically, the arising signals have to be calculated on the basis of an appropriate model, e.g. the signal modeling described be de Groot and de Lega.[10] However, this is not the intention of this paper. Nevertheless, a theoretical understanding of the phenomenon, which is relevant in this context, can be obtained from an approach published by Pförtner and Schwider.[8]

If a two-beam interference is assumed, the following equation for the interference intensity holds:

$$I(z_0) = I_0 \, V \cos(k \, z_0), \tag{1}$$

with the wavenumber $k = 2\pi/\lambda$, the corresponding surface height value $z_0/2 = h$, the visibility V, and the mean intensity I_0. In order to calculate the interference intensity of a broadband light source, one has to integrate over the wavenumber k. If a Gaussian spectral distribution of the wavenumber with the mean value $\bar{k}$ and the spectral width Δk is assumed and, in addition, a dispersion showing a linear wavenumber dependence controlled by a parameter c the following equations hold:

$$I(z_0) = I_0\, V \int_{-\infty}^{+\infty} \exp\left(-\frac{(k-\bar{k})^2}{\Delta k^2}\right) \cos\left(k\, z_0 + (k-k_0)\, c\right) \mathrm{d}k \tag{2a}$$

$$= I_0\, V\, \mathrm{Re}\left\{ \int_{-\infty}^{+\infty} \exp\left(-\frac{(k-\bar{k})^2}{\Delta k^2}\right) \exp\left(i\, k\, z_0 + i\,(k-k_0)\, c\right) \mathrm{d}k \right\} \tag{2b}$$

$$= I_0\, V\, \mathrm{Re}\left\{ \exp\left(-i\, k_0 c\right)\, \mathrm{FT}_{\mathrm{k}}^{-1}\left\{ \exp\left(-(k-\bar{k})^2 / \Delta k^2\right) \exp\left(i\, k\, c\right) \right\} \right\} \tag{2c}$$

$$= I_0\, V\, \sqrt{\pi}\, \Delta k \exp\left(-(z_0 + c)^2\, \Delta k^2 / 4\right) \cos\left(\bar{k} z_0 - (k_0 - \bar{k})\, c\right). \tag{2d}$$

The interference intensity I as a function of twice the scanner position $z_0/2$ related to equal optical path lengths is the real part of the inverse Fourier transformation of the Gaussian distribution multiplied by the phase term $\exp(i\, k\, c)$, the complex constant $\exp(-i\, k_0\, c)$, the mean intensity I_0, and the visibility V (see eq. 2c). A phase shift in the Fourier domain results in a shift of the axial position of the Fourier transformed spectral distribution (see eq. 2d). Therefore, dispersion leads to a shift of the coherence peak position. The high frequency interference term depends on the mean wavenumber $\bar{k}$ of the spectral distribution. The above equation shows, that, if the wavenumber k_0 equals $\bar{k}$, there is no influence of the dispersion on the phase of the signal.

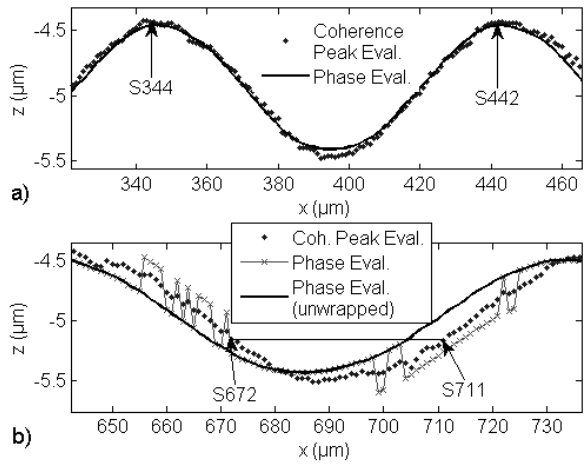

Figure 9: a) Detail of Fig. 6 a) showing the results of coherence peak and phase evaluation in the middle of the field of view, b) Detail of Fig. 6 a) showing the results of coherence peak, phase, and unwrapped phase evaluation close to the edge of the field of view.

The above statements can be tested by considerations similar to the procedure described by Sinclair et al.[11] in order to compensate for dispersion effects in a Linnik white-light interferometer. Figure 9 shows sections of the calculated surface profiles according to Fig. 6 a). In Fig. 9 a) two sample points corresponding to the signals at x = 344, and 442 µm, respectively are chosen, for which the result of the coherence peak evaluation leads to nearly the same surface height value. The power spectral density curves according to Fig. 10 a), which are attributed to these signals are also nearly identical. Since the slope of the phase of a SWLI signal in the Fourier domain is strongly correlated to the position of the coherence peak on the height axis,[1] the slope of the phase values according to Fig. 10 b) doesn't differ significantly for the two signals. However, the situation is different if two signals arising at the flanks close to the edge of the field of view are compared. Appropriate signals are located at x positions 672 µm and 711 µm in Fig. 9 b). Again the surface height obtained from coherence peak evaluation is nearly the same for these two positions, but a maximum dispersion difference is to be expected according to the model of Fig. 8 and ghost steps occur in Fig. 9 b). The power spectral density curves and the phase spectra for these signals are plotted in Fig. 10 c) and d), respectively. In the vicinity of the spectral peak the phase slope is again nearly the same for the two signals. The difference in phase slope between Fig. 10 b) and d) is associated with the different coherence peak positions. The dispersion phenomenon becomes visible in Fig. 11, where the differences of the phase spectra for the two signal pairs according to Fig. 10 b) and d) are displayed. For the signals 344 and 442, where no dispersion difference is to be expected, the resulting phase difference curve in Fig. 11 is approximately constant. For the signals 672 and 711, where the dispersion difference should be significant, i.e. the group velocity changes with the wavenumber k, an approximately parabolic curve shape results, which confirms the above considerations.

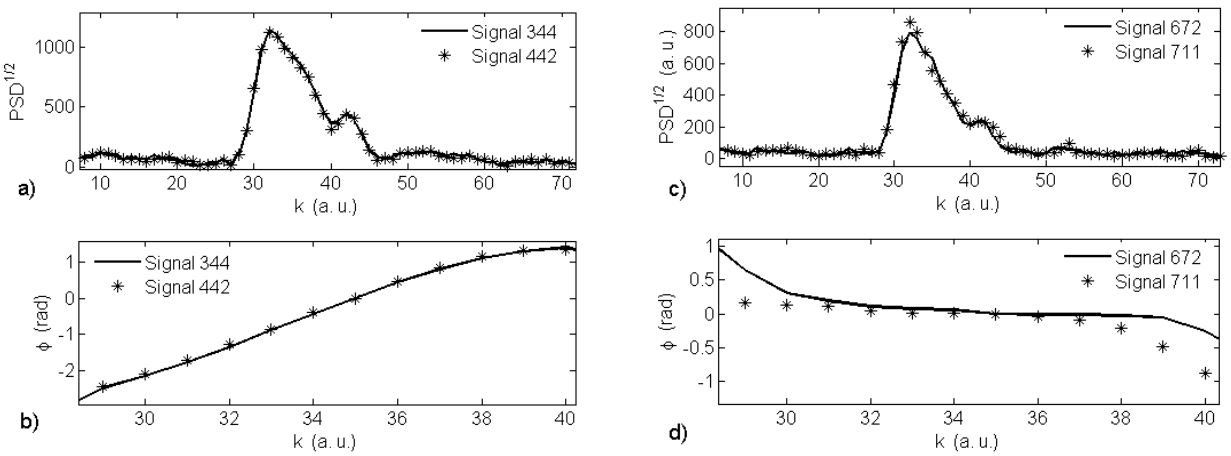

Figure 10: a) Power spectral density curves of the signals marked in Fig. 9 a), b) unwrapped spectral phase curves in the vicinity of the spectral maxima according to a), c) power spectral density curves of the signals marked in Fig. 9 b), d) unwrapped spectral phase curves in the vicinity of the spectral maxima according to c).

As a consequence of the interpretation of the measuring results obtained from the sinusoidal surface, ghost steps should also occur for an optical flat, which is tilted with respect to the optical axis of the SWLI sensor. A result of such a measurement is plotted in Figure 12. The profiles according to Fig. 12 a) were taken in the direction of maximum surface tilt. The tilt angles obtained from coherence peak and (unwrapped) phase evaluation are different. This becomes more obvious, if one looks at the difference curves shown in Fig. 12 b). (The high frequency oscillation comes from vibrations in the surrounding, see Fig. 3.) The surface slope was 4.6°. Close to the left edge of the diagram the situation of perpendicular incidence according to Fig. 8 d) can be found in a decrease of the deviation between coherence peak and phase evaluation. Finally, the differences between phase evaluation based on the fringe order determination by use of the coherence peak and unwrapped phase evaluation exhibits several ghost steps in Fig. 12 b).

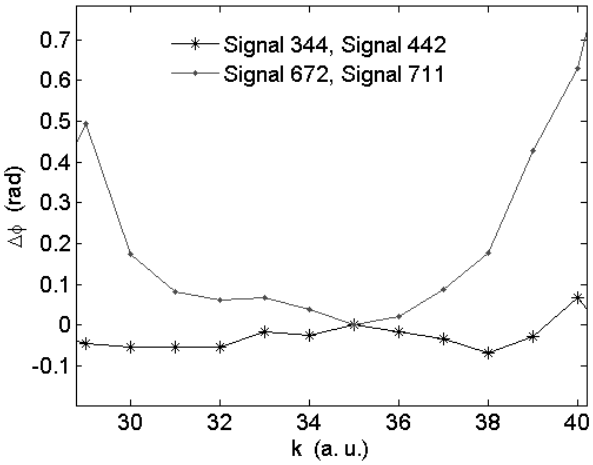

Figure 11: Spectral curves showing the phase difference of the results according to Fig. 8 b) and 8 d).

6. CONCLUSIONS AND OUTLOOK

It was shown, that dispersion differences of two interfering light rays in a Mirau interferometer depend on the local surface slope and the position at any point within the field of view. The deviations between the height values obtained from the coherence peak and those obtained from phase evaluation are strongly related to the radial distance of the point of observation from the optical axis in the case of surface slopes.

Furthermore, it seems that these dispersion effects also influence the occurrence of batwings. As it can be obtained from Fig. 4 a) and b), the batwing effect shows a strong dependence on the position within the field of view, i.e. the distance between the optical axis and the observation point.

Another situation, where the dispersion effect, which arises from local surface slopes, influences the measuring result can be observed in Fig. 3 and Fig. 5 a), c). The sub-microstructure, e.g. the grain boundaries, yield to greater height differences, if the coherence peak is evaluated, whereas these height differences seem smaller, if the phase of the signal

is analyzed. This phenomenon of an enhanced microstructure can be generally observed in SWLI measurements based on coherence peak evaluation. It may be interpreted as an increased measuring uncertainty.[12]
Another effect, we observed in our measurements was, that the amplitudes of a sinusoidal surface obtained from coherence peak evaluation are generally slightly greater than those obtained by phase evaluation (see Fig. 9 (a)). The reason for this could be a dispersion difference in measurement and reference beam caused by the focusing / defocusing resulting from the curvature of the sinusoidal grooves.
An approach to minimize the dispersion effects could be a reduction of the thickness of the plane glass plates used in the Mirau objective. In order to check this, SWLI measurements using a Mirau objective of a different manufacturer were

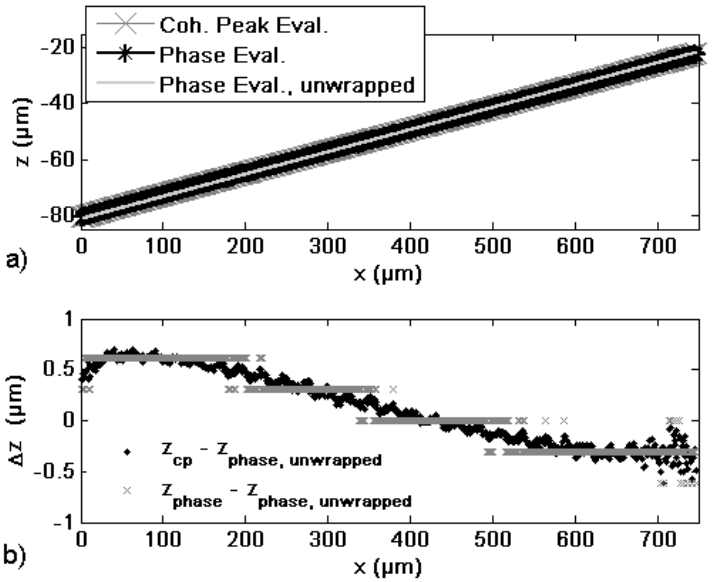

Figure 12: a) SWLI measurement results for a tilted flat measuring object showing a different slope of the coherence peak and the (unwrapped) phase evaluation; b) calculated height difference curves for coherence peak and (unwrapped) phase evaluation (continuous curve) as well as for phase difference curves with and without unwrapping (step like curve).

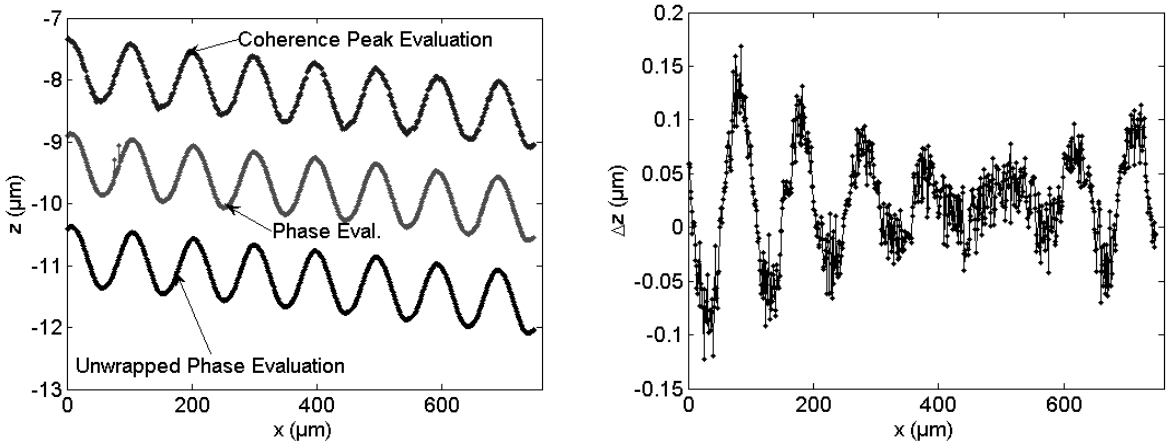

a) **b)**

Figure 13: a) Sinusoidal profiles with 0.5 µm amplitude and 100 µm period length obtained from coherence peak evaluation only (a), top), from coherence peak evaluation followed by phase evaluation (a), middle), and from phase evaluation followed by phase unwrapping (a), buttom), and b) difference between coherence peak and unwrapped phase evaluation, results obtained with a Mirau objective from a different manufacturer compared to the results shown in Fig. 4 but with the same parameters (20x, 0.4).

carried out without any further changes of the experimental setup. Results are shown in Fig. 13. Since the glass plates were thinner, in comparison with Fig. 6 b) the dispersion effect is smaller in Fig. 13 b). However, the principal shape of the curve showing the discrepancies is nearly the same as in Fig. 6 b). Consequently, a reduction of the thickness of the glass plates within the Mirau objective shifts the occurrence of ghost steps to higher tilt angles or greater distances from the optical axis.
Another approach, which will be realized soon, is to use a two-wavelength SWLI configuration in order to extend the range of unambiguousness by use of a phase evaluation technique based on a synthetic wavelength.
Nevertheless, the study presented here, contributes to a deeper understanding of phenomena emerging if white-light interferometry is applied to measure the geometry of MEMS or MOEMS. Hence, it builds the basis to overcome some of the current limitations of SWLI in near future.

ACKNOWLEDGEMENT

The support of this work by the German ministry of education and research (BMBF) under project No. 16SV1942 is gratefully acknowledged.

REFERENCES

1. P. de Groot, L. Deck, "Surface profiling by analysis of white-light interferograms in the spatial frequency domain," *J. of Mod. Opt.* **42**, 389-401, 1995.
2. B. S. Lee, T. C. Strand, "Profilometry with a coherence scanning microscope," *Appl. Opt.* **29**, 3784- 3788, 1990.
3. M. Fleischer, R. Windecker, H. J. Tiziani, "Fast algorithms for data reduction in modern optical three-dimensional profile measurement systems with MMX technology," *Appl. Opt*. **39**, 1290-1297, 2000.
4. A. Harasaki, J. Schmit, J. C. Wyant, "Improved vertical-scanning interferometry," *Appl. Opt.* **39,** 2107-2115, 2000.
5. P. de Groot, X. Colonna de Lega, J. Kramer, M. Turzhitsky, "Determination of fringe order in white-light interference microscopy," *Appl. Opt*. **41**, 4571-4578, 2002.
6. A. Harasaki, J. C. Wyant, "Fringe modulation skewing effect in white-light vertical scanning interferometry," *Appl. Opt*. **39,** 2101-2106, 2000.
7. K. Creath, "Calibration of numerical aperture effects in interferometric microscope objectives," *Appl. Opt.* **28**, 3333 - 3338, 1989.
8. A. Pförtner, J. Schwider, "Dispersion error in white-light Linnik interferometers and its implications for evaluations procedures," *Appl. Opt*. **40**, 6223-6228, 2001.
9. J. Schmit, A. Olszak, "High-precision shape measurement by white-light interferometry with real-time scanner error correction," *Appl. Opt*. **41**, 5943-5950, 2002.
10. P. de Groot, X. Colonna de Lega, "Signal modeling for low-coherence height-scanning interference microscopy," *Appl. Opt*. **43**, 4821-4830, 2004.
11. M. B. Sinclair, M. P. de Boer, A. D. Corwin, "Long-working-distance incoherent-light interference microscope," *Appl. Opt*. **44**, 7714-7721, 2005.
12. H. G. Rhee, T. V. Vorburger, J. W. Lee, and J. Fu: "Discrepancies between roughness measurements obtained with phase-shifting and white-light interferometry," *Appl. Opt*. **44**, 5919-5927, 2005.